Computers and Electronics in Agriculture 189 (2021) 106421

Contents lists available at ScienceDirect

Computers and Electronics in Agriculture

journal homepage: www.elsevier.com/locate/compag

Original papers

Estimation of nitrogen nutrition index in rice from UAV RGB images coupled with machine learning algorithms

Zhengchao Qiu [a,b], Fei Ma [a], Zhenwang Li [a], Xuebin Xu [a], Haixiao Ge [a,b], Changwen Du [a,b,*]

[a] The State Key Laboratory of Soil and Sustainable Agriculture, Institute of Soil Science Chinese Academy of Sciences, Nanjing 210008, China
[b] College of Advanced Agricultural Sciences, University of Chinese Academy of Sciences, Beijing 100049, China

ARTICLE INFO

Keywords:
Rice
Nitrogen nutrition index
Unmanned aerial vehicle
Machine learning
Precision fertilization

ABSTRACT

Rapid and accurate estimation of rice Nitrogen Nutrition Index (NNI) is beneficial for management of nitrogen application in rice production. Traditional estimation methods required manual actual measurement data in the field, which was time-consuming and cost-expensive, and RGB images from unmanned aerial vehicle (UAV) provided an alternative option for nitrogen nutrition index (NNI) monitoring. In this study, RGB images from unmanned aerial vehicle (UAV) were obtained from each growth period of rice, and six machine learning (ML) algorithms, i.e., adaptive boosting (AB), artificial neural network (ANN), K-nearest neighbor (KNN), partial least squares (PLSR), random forest (RF) and support vector machine (SVM), were used to extract target information for estimating NNI as well as vegetation index (VI). Results showed that most UAV VIs were significantly correlated with rice NNI at the key growing periods; the estimation results of rice NNI using six ML algorithms showed that the RF algorithms performed the best at each growth period with the determination coefficient (R^2) ranged from 0.88 to 0.96 and room mean square error (RMSE) ranged from 0.03 to 0.07, in which the estimation of NNI was the best in filling period and the early jointing stage. Rice NNI at the early jointing stage was significantly correlated with soil available nitrogen (AN) with the R^2 of 0.84 in Pukou and 0.72 in Luhe, respectively, and rice NNI was significantly correlated with the yield with the R^2 of more than 0.7 in Pukou at the whole period and more than 0.7 in Luhe from late jointing to maturity stage. Therefore, the combination of RGB images from UAV and ML algorithms was a scalable, simple and inexpensive method for rapid qualification of rice NNI, which effectively improved nitrogen use efficiency and provided guidance for precision fertilization in rice production.

1. Introduction

Rice is a major food crop in China and plays an important role in food security, and nitrogen (N) application is one of the key factors in the rice yield, but N use efficiency is low as around 30%, which resulted in arable land degradation and water eutrophication (Wu and Ma, 2015). Nitrogen status is an important indicator for monitoring rice growth and estimating yield, and timely monitoring of rice nitrogen status in the field could benefit precision nitrogen application and yield improvement (Shi et al., 2021).

The conventional way of monitoring rice nitrogen status required manual actual sampling in field and physicochemical analysis in laboratory, which was time-consuming, labor-intensive, and costly (Cohan et al., 2019), and thereof was difficult to apply at all growth stages of the crop. With the development of modern technology, portable instruments were used to measure key growth indicators of crops (Sankaran et al.,

Abbreviations: AB, adaptive boosting; AGB, aboveground biomass; AN, available nitrogen; ANN, artificial neural network; DN, digital number; DNG, double-negative group; ExB, excess blue vegetation index; ExG, excess green vegetation index; ExGR, excess green minus excess red; ExR, excess red vegetation index; GLA, green leaf algorithm; GLI, green leaf index; GRVI, green red vegetation index; JPEG, joint photographic experts group; KNN, K-nearest neighbor; MGRVI, modified green red vegetation index; ML, machine learning; MLR, mixed logistic regression; N, nitrogen; N_a, the measured N concentration; N_c, N content; NDVI, normalized difference vegetation index; NNI, nitrogen nutrition index; PLSR, partial least squares regression; R^2, coefficient of determination; RF, random forest; RGBVI, red green blue vegetation index; RGRI, red green ratio index; RMSE, room mean square error; ROI, region of interest; RVI, ratio vegetation index; SVM, support vector machine; UAV, unmanned aerial vehicle; VARI, visible atmospherically resistant index; VI, vegetation index.

* Corresponding author at: The State Key Laboratory of Soil and Sustainable Agriculture, Institute of Soil Science Chinese Academy of Sciences, Nanjing 210008, China.
E-mail address: chwdu@issas.ac.cn (C. Du).

https://doi.org/10.1016/j.compag.2021.106421
Received 20 February 2021; Received in revised form 24 August 2021; Accepted 25 August 2021
Available online 31 August 2021

2015), such as active canopy sensor GreenSeeker (Trimble Inc., Sunnyvale, CA, USA), which could obtain the normalized difference vegetation index (NDVI) and greenness vegetation index (RVI) using optic scanning method in the visible and near-infrared range. The SPAD (Minolta Camera Co., Osaka, Japan) meter was used to quickly measure the relative chlorophyll content of plant leaves, and the connection with nitrogen status improved nitrogen management in crop production (Singh et al., 2016). Digital photos were used to obtain crop canopy cover, and a new method of nitrogen nutrition index (NNI) acquisition was established by using canopy cover instead of crop dry biomass (Wang et al., 2016). The method was proved to be as accurate as using crop aboveground biomass (AGB) to obtain NNI; while avoiding the drawbacks when obtaining crop dry biomass through sampling (Shi et al., 2021). These optical instruments could obtain crop growth information quickly, i.e., proximate sensing, but professional and mass onsite measurements were needed, which made it limited in large-scale applications. Remote sensing is another method to cope with the problems raised in proximate sensing. Remote sensing by satellites was used to estimate crop growth indicators, which provided solutions for application over a large area; however, satellites based remote sensing was easily impacted by the weather conditions, and also showed obvious time and resolution limitations (Kogan, 2007), which made it difficult to serve in practice, and UAV provided an alternative option for remote sensing.

Many studies showed that UAV could be used to achieved in monitoring crop growth, and for UAV monitoring light source was one of key factors in estimating key crop growth parameters (Li et al., 2015). Hyperspectral cameras with the hundreds of narrow spectral bands could provide users with the rich sources of information, and multispectral cameras were shown to be very important in estimating key crop growth parameters (Kerkech et al., 2020). Compared to these cameras, RGB cameras have the advantage of being more economic (Wang et al., 2013), and it was also possible to extract important VIs from these UAV images to achieve the estimation of crop growth parameters (Yang et al., 2019). Therefore, it was feasible to use UAVs with low-cost RGB cameras for monitoring NNI in rice production.

A single VI extracted from UAV-RGB images resulted from limited band information, and in order to make full use of the information in each band of the image, multiple VIs and machine learning (ML) algorithms with UAV remote sensing technology could be combined to predict crop growth parameters (Han et al., 2019). Regarding the use of UAV imagery to achieve estimation of crop growth indicators, these algorithms resulted in well performance (Lu et al., 2019). There were many ML algorithms (e.g., multiple linear regression, SVM, ANN, and RF), which showed different performances in crop monitoring using UAV (Han et al., 2019), and it was needed to optimize the ML algorithms in monitoring rice NNI for practical applications.

It was widely recognized that NNI showed great potential for N status assessment, thereof it was used as an important indicator to guide variable fertilization (Shi et al., 2021); during the crop growth, the application of nitrogen is one of the important factors affecting crop yield, and also determines the content of grain protein, which affects the crop quality. The soil AN was a direct indicator to evaluate the soil N fertility (Ma et al., 2017); however, the relationship between NNI and soil AN remains unclear. Therefore, the use of UAV to diagnose the nitrogen status of rice, including the relationship between the NNI of the aboveground crops and the nitrogen content in the soil, could achieve better guidance for the reasonable application of nitrogen fertilizers while improving crop yield and quality.

Therefore, the objectives of this study are to (1) explore the possibility of UAV-RGB images applied in estimation of NNI in rice production; (2) optimize the ML algorithm for estimating NNI of rice; (3) verify the accuracy of estimated NNI through the relationship between NNI and rice yield, NNI and soil AN in practical rice production.

2. Materials and methods

2.1. Experimental design descriptions

There were two experimental fields involved in this study, located in Pukou District and Luhe District, Nanjing, Jiangsu province, China ($32^{\circ}04'15''N$, $118^{\circ}28'21''E$ and $32^{\circ}25'4''N$, $118^{\circ}59'18''E$, respectively) (Fig. 1), which were in tropical humid climate region with an average annual temperature of 15.4 °C, a maximum annual temperature of 39.7 °C, and a minimum temperature of −13.1 °C. Each experiment was set into plots for treatments with replications regarding the rates and types of input N (Table1), i.e., 5 treatments considering the rates of controlled release fertilizer input with 4 replications (20 plots) for Pukou experiment, and 4 treatments with 4 replications (three replications for CK, totally 15 plots, each plot 200 m^2) for Luhe experiment.

The soil type in Pukou experiment was paddy soil (anthrosol) with 22.26 g kg^{-1} organic matter, 1.31 g kg^{-1} total N, 15.41 mg kg^{-1} Olsen-P, and 146.4 mg kg^{-1} available K. The soil in Luhe experiment was also anthrosol with 26.56 g kg^{-1} organic matter, 1.58 g kg^{-1} total N, 15.21 mg kg^{-1} Olsen-P, and 166.2 g kg^{-1} available K. A japonica rice cultivar with strong resistance to diseases called Nanjing 5055 in both experiments was transplanted in June and harvested on November 2019.

2.2. Crop and soil data acquisition

The key growth period of rice was selected for plant and soil sample collection (Table 2), and three representative holes plant were selected from each experimental plot as the sample and placed in a plastic sealed bag for laboratory processing. The rice shoots were dried at 80 °C to a constant weight as the AGB, and total N content in rice shoots were determined using the Kjeldahl method (Nelson and Sommers, 1973). At the same time, 0–20 cm topsoil were collected, and Soil AN was measured using the Kjeldahl method (Table 2).

2.3. Yield data acquisition

In the Pukou experimental field, rice in each plot was completely harvested, threshed and weighed to obtain the total weight. The moisture content was determined with a grain moisture tachometer, and the average value was obtained by repeating three times. One square meter was randomly selected to determine the impurity rate and empty defoliation rate. In the Luhe experimental field, 3 square meters of rice were randomly selected within each ROI for manual cutting. Then obtaining the total weight, the moisture content the impurity rate and deflated rate using the same method as Pukou yield measurement. In all fields, the standard dry weight moisture content of rice was selected as 14.5%.

2.4. Calculation of nitrogen nutrient index

Nitrogen nutrient index (NNI) is the ratio between aboveground biomass of rice and critical N concentration, which describes the nitrogen status of rice, independent of growth stage and different biomass. NNI values close to 1 indicate that rice has optimal N supply, NNI > 1 indicates excessive N supply, and NNI < 1 indicates N deficiency (Fabbri et al., 2020). Table 2 presents the descriptive statistics of the rice NNI at different stage of rice growth.

The critical N content (N_c) of rice was described by the following equation (1) (Wang et al., 2016):

$$N_c = 3.33AGB^{-0.26} \quad (1)$$

Where N_c was the critical N content as a percentage of dry biomass and AGB was the dry weight of above ground biomass in mg/ha.

The NNI was calculated using Equation (2)

$$NNI = N_a/N_c \quad (2)$$

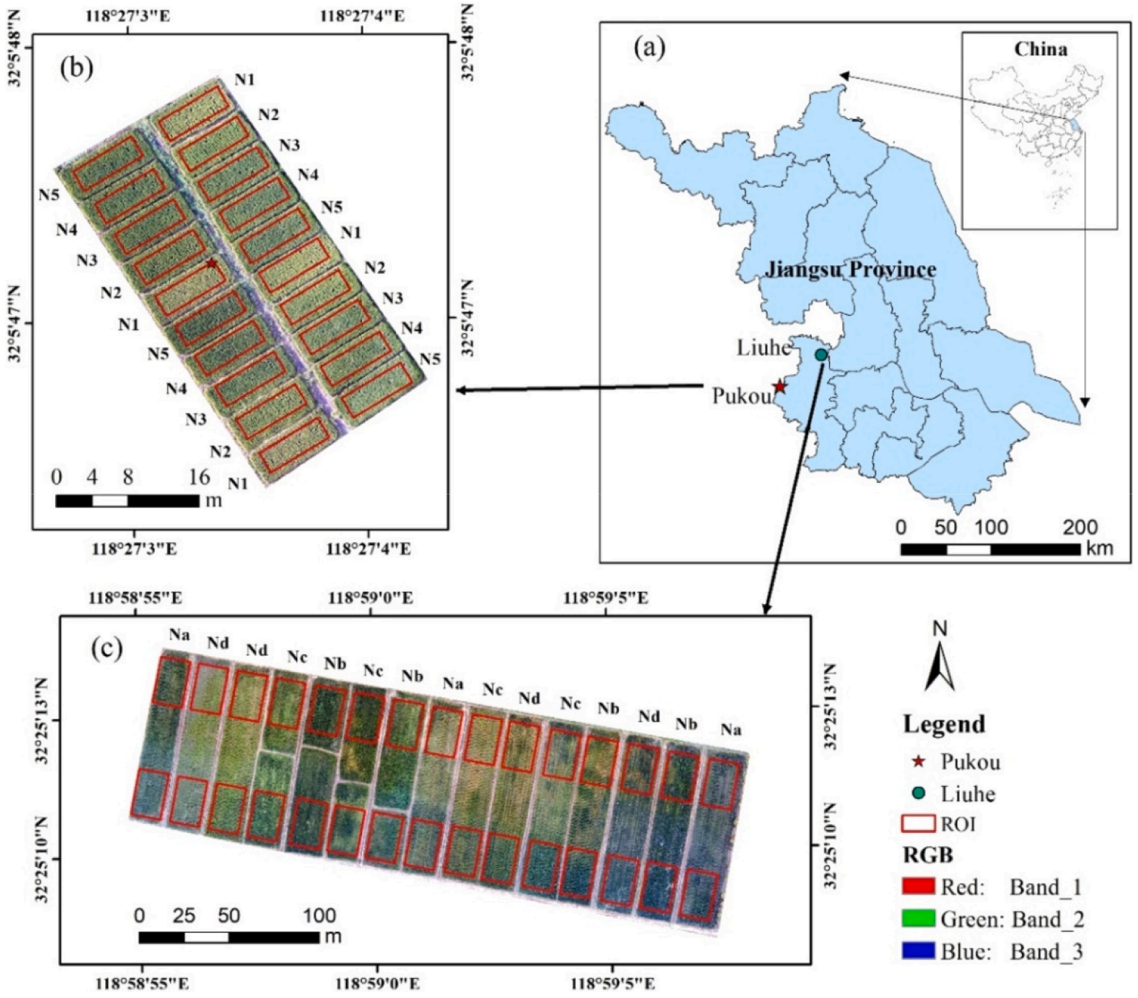

Fig. 1. Geographic location of the research area and UAV images of the experimental plots with different fertilization treatments (a, The location of Jiangsu Province in China and the location of Pukou and Luhe experimental stations; b, An UAV image of Pukou experimental plots with 5 fertilization treatments and regions of interest for sampling and VI extraction; c, An UAV image of Luhe experimental plots 4 fertilization treatments and regions for sampling and VI extraction).

Table 1
Fertilization treatments in the field experiment of rice.

experimental field	Fertilization treatments	Compound fertilizer (kg)	Proportion of controlled release N
Pukou	N1	0	0
	N2	240 kg ha^{-1}	0
	N3	240 kg ha^{-1}	30%
	N4	240 kg ha^{-1}	40%
	N5	240 kg ha^{-1}	50%
Luhe	Na	196 kg ha^{-1}	0
	Nb	196 kg ha^{-1}	50%
	Nc	176 kg ha^{-1}	50%
	Nd	158 kg ha^{-1}	50%

Note: Coated urea (N, 42%) was used as controlled release N, and was produced by Jiangsu ISSAS Fertilizer Corporation, Yizheng, China).

Where N_a was the measured N concentration.

2.5. Acquisition of UAV images

The Phantom 4 Professional UAV (SZ DJI Technology Co., Shenzhen, China) was used to obtain high spatial resolution images of the two experimental fields at each sampling period. The UAV platform installed with a 20 million pixel visible light (RGB) camera. Aerial photographs of the experimental fields were captured using the UAV flying at a height of 100 m from the ground at a speed of 8 m/s. The side and forward overlap properties of the image were set to 60–80%. Every flight was carried out in clear, cloudless, and windless weather. The images were automatically captured, with one frame every 2 s, in joint photographic experts group (JPEG) and double-negative group (DNG) formats between 11:00 and 13:00. Considering the RGB camera reflectivity correction, three diffuse reflective plates (Guangzhou Changhui Electronic Technology Co., Ltd.) were placed on the ground while the UAV flying, with reflectivity of 10%, 50% and 90% respectively.

2.6. UAV image processing and index extraction

The Pix4Dmapper (https://www.pix4d.com/) was used to generate orthophoto images of the acquired images. In this process, Pix4Dmapper opened all photos taken during the same period according to the location coordinates in their attributes; the software automatically aligns the overlapping images using a feature point matching algorithm. Then, 10 evenly distributed ground control points were used to georeference each image for alignment. In Pix4Dmapper, internal camera parameters were estimated based on photo alignment and the location of ground control points. A sharp depth filter was selected and reconstructed small details to build a dense point cloud. Finally, the default parameters were used to build the mesh and textures to generate the orthophoto and export it as a TIFF image. The radiation calibration is performed by the method of calibration plates, and the image values were converted into image

Table 2
Descriptive statistics of the NNI, AN at different stage of rice growth and yield.

	Date	Mean	Median	SD	Variance	Kurtosis	Skewness	Min	Max
NNI	Tillering stage	1.02	1.02	0.22	0.05	1.04	0.04	0.52	1.63
	Early jointing	0.90	0.94	0.22	0.05	−0.11	−0.24	0.44	1.34
	End of jointing	0.89	0.91	0.24	0.06	−0.70	−0.11	0.44	1.44
	Booting stage	0.85	0.85	0.24	0.06	−0.46	−0.15	0.36	1.39
	Blooming period	0.65	0.65	0.15	0.02	0.01	0.26	0.38	1.07
	Grouting period	0.59	0.58	0.16	0.03	−0.31	0.43	0.30	0.97
	Maturity	0.55	0.55	0.12	0.02	−0.76	0.24	0.34	0.78
AN (mg kg^{-1})	Tillering stage	42.06	42.72	20.59	424.0	−1.05	0.30	12.58	87.97
	Early jointing	24.29	21.45	12.21	149.02	−0.78	0.57	7.21	49.43
	End of jointing	25.51	24.28	9.30	86.53	−0.42	0.63	11.56	49.77
	Booting stage	16.77	15.11	5.87	34.45	3.35	1.78	10.01	36.57
	Blooming period	15.42	14.31	4.02	16.17	0.12	0.55	7.18	26.38
	Grouting period	6.50	6.03	1.63	2.66	−0.19	0.39	3.10	10.48
	Maturity	13.90	13.95	2.34	5.48	0.98	0.77	9.56	20.44
Yield (kg $acre^{-1}$)		494.4	531.9	111.3	12388.3	−0.82	−0.59	243.6	640.7

reflectance by the reflectance of the ground reflective plates; thus, the surface reflectance was reflected in real time. The formula of radiation calibration was described by the following equation (3) to equation (5):

$$R_i = gain \times DN_i + offset \tag{3}$$

$$gain = \frac{R_{max} - R_{min}}{DN_{max} - DN_{min}} \tag{4}$$

$$offset = R_{min} \tag{5}$$

Where R_i was the reflectance of the i-th band, *gain* was the incremental correction coefficient, *offset* was the correction deviation, DN_i was the grayscale value of the i-th band, DN_{max} and DN_{min} were the maximum and minimum grayscale values of the UAV image, R_{max} was the maximum reflectance of the calibration plate, and R_{min} was the minimum reflectance of the calibration plate.

The reflectance values of the red (r), green (g), and blue (b) bands of the UAV images in each field were extract. Then Python3.7.8 (https://www.python.org/) was used to calculate the corresponding VI (Table 3). ArcGIS10.3 (https://www.esri.com) was used to draw the region of interest (ROI) (Fig. 1) in the center of each plot and the average value of various VIs was extracted at different periods in each ROI as the VI of each plot.

Table 3
List of vegetation indices (VIs) used in this study.

Name	Index	Formulation	References
Green Leaf algorithm	GLA	(2*g-r-b)/(2*g + r + b)	(Louhaichi et al., 2008)
Green Leaf Index	GLI	(2*g-r + b)/(2*g + r + b)	(Louhaichi et al., 2008)
Green Red Vegetation Index	GRVI	(g-r)/(g + r)	(Tucker, 1979)
Modified Green Red Vegetation Index	MGRVI	$(g^2\text{-}r^2)/g^2 + r^2)$	(Bendig et al., 2015)
Excess Green minus Excess Red	ExGR	(2*g-r-b)-(1.4*r-g)	(Yang et al., 2019)
Excess Red Vegetation Index	ExR	1.4*r-g	(Meyer and Neto, 2008)
Excess Blue Vegetation Index	ExB	1.4b-g	(Qi et al., 1994)
Excess Green Vegetation Index	ExG	2*g-r-b	(Woebbecke et al., 1995)
Visible Atmospherically Resistant Index	VARI	(g-r)/(g + r-b)	(Saberioon and Gholizadeh, 2016)
Red Green Blue Vegetation Index	RGBVI	$(g^2\text{-}b*r^2)/(g^2 + b*r^2)$	(Possoch et al., 2016)
Red Green Ratio Index	RGRI	r/g	(Verrelst et al., 2008)

Note: r, g and b represent the reflectance values of the red, green, and blue bands of the UAV images, respectively, the same below.

2.7. Machine learning algorithms

Various machine learning algorithms, including adaptive boosting (AB), artificial neural network (ANN), K-nearest neighbor (KNN), partial least squares (PLSR), random forest (RF), and support vector machine (SVM), were used to evaluate the performance of the ML model for rice NNI based on VIs from UAV images (Scornet, 2015).

2.8. Model evaluation

For the six ML algorithms in this study, 70% data was selected for training and 30% data for testing. For the estimated rice NNI using the best ML algorithms, the measured NNI was used to validate the estimated NNI extracted from the ROIs of each plot. Coefficient of determination (R^2) and root mean square error (RMSE) were calculated to verify the reliability of the model. These parameters were calculated as follows:

$$R^2 = \frac{\sum_{i=0}^{n}(X_i - \overline{X})^2(Y_i - \overline{Y})^2}{n\sum_{i=0}^{n}(X_i - \overline{X})^2\sum_{i=0}^{n}(Y_i - \overline{Y})^2} \tag{6}$$

$$RMSE = \sqrt{\frac{1}{n}\sum_{i=1}^{n}(Y_i - X_i)^2} \tag{7}$$

Where X_i and Y_i were estimated NNI and measured NNI, respectively, $\overline{X}$ and $\overline{Y}$ were the average estimated NNI and measured NNI, respectively, and n was the number of samples.

3. Results

3.1. Relationship between UAV-VIs and NNI

Correlation coefficients were calculated between the eleven VIs extracted from the UAV images and NNI in different growth periods (Table 4). At different growth periods, the VIs with the best correlation to NNI varied. The best VI was RGRI with R^2 of 0.61 at tillering stage, the best correlation between ExR and NNI at the early stage of jointing with R^2 of 0.59. The correlation coefficients (R^2) between VARI and NNI at the late jointing and booting stage were 0.55 and 0.60, respectively. At flowering, filling and maturity stages, three optimal UAV-Vis, i.e., GRVI, MGRVI and RGRI, showed the significant correlations with rice NNI, which demonstrated that these UAV-VIs could be used to estimate the NNI of rice.

3.2. NNI estimations using different ML algorithms

NNI was predicted from UAV-Vis at different growth stage using six

Table 4
Correlation of rice NNI with UAV-VIs at different growth stage.

VI	Tillering	Early jointing	Late jointing	Booting	Flowering	Filling	Maturity
ExB	0.06	0.19	0.06	0.46***	0.19	0.05	0.35*
ExGR	0.06	0.43**	0.07	0.12	0.43**	0.49***	0.25*
ExG	0.15	0.38**	0.20	0.12	0.15	0.19	0.08
ExR	0.04	**0.59*** **	0.44**	0.54***	0.60***	0.44**	0.73***
GLA	0.24*	0.28*	0.36*	0.05	0.19	0.55***	0.08
GLI	0.28*	0.30*	0.45**	0.02	0.20	0.56***	0.08
GRVI	0.60***	0.44**	0.50***	0.46***	**0.61*** **	**0.79*** **	**0.67*** **
MGRVI	0.60***	0.43**	0.48***	0.46***	**0.61*** **	**0.79*** **	**0.67*** **
RGBVI	0.06	0.16	0.39**	0.08	0.35*	0.63***	0.02
RGRI	**0.61*** **	0.42**	0.48***	0.45***	**0.61*** **	**0.79*** **	**0.67*** **
VARI	0.57***	0.48***	**0.55*** **	**0.60*** **	0.54***	0.78***	0.61***

* 10% level of significance with p-values between 0.05 and 0.1; ** 5% level of significance with p-values between 0.01 and 0.05; *** 1% level of significance of significance with p-values less than 0.01

ML algorithms (AB, ANN, KNN, PLSR, RF and SVM) (Table 5). RF model showed the highest accuracy in estimating NNI with R^2 ranging from 0.88 to 0.97, and RMSE ranging from 0.03 to 0.07 from tillering to maturity stage. Except the AB algorithm, all other ML algorithms showed the highest estimation accuracy at filling stage, followed by early jointing stage, among which RF algorithm was optimal when using UAV RGB images for rice NNI estimation.

Fig. 2 shows the validation results of different ML for rice NNI estimation at different growth periods. In the picture, different colors represent different ML estimation models, and the seven growth periods were evenly distributed around the circles. From the center of the circle to the outside, the value gradually became larger. Connecting the validation results of each ML in the whole growth period, the closer shape to a circle indicated more stable model. In the R^2 plot, the larger shape showed better model accuracy; and in the RMSE plot, the smaller shape demonstrated the smaller estimation error. It was obviously observed that RF was the optimal ML algorithms for estimating rice NNI, R^2 was greater than other models in each growth period, and RMSE was smaller than other ML algorithms. The KNN algorithms showed the worst performance among all models with the validated R^2 of less than 0.60 in all growth periods.

3.3. The correlation between yield and NNI

The correlations between yield and NNI at different periods in Luhe and Pukou were showed in Fig. 3. The NNI and yield in Pukou experimental field were significantly correlated throughout the growing season, and the correlation coefficients were greater than 0.80 in the early jointing, late jointing, flowering and filling periods. NNI in Luhe experimental field were significantly correlated to yield from the early jointing period to maturity period, and the correlation coefficients in the late jointing and filling periods were greater than 0.80; in other periods, the correlation coefficients in the Luhe were smaller than those in the Pukou, which might be due to the farmland scale; the relationships between NNI and yield in both experimental fields were highest at the late jointing and the filling stage, indicating that the high or low NNI of rice during these two growth periods affected the yield status.

3.4. Correlation between NNI and soil AN

Fig. 4 shows the correlation matrix of rice NNI at different periods with the soil AN at the corresponding periods. The correlation between the NNI and soil AN was the highest at the jointing stage in the Luhe experimental field with a correlation coefficient of 0.72; followed by the maturity stage, with a correlation coefficient of 0.71 (Fig. 4b). In the Pukou experimental field, the correlation between the NNI and soil AN was the highest at the jointing stage with a correlation coefficient of 0.84 (Fig. 4b); the correlation coefficient at the tillering stage was the second highest with a correlation coefficient of 0.77. It was found that there is a stable and significant correlations between the rice NNI and soil AN at the jointing period.

3.5. Accuracy assessment of NNI prediction

From Fig. 5a, it was observed that the NNI of rice was very low, mostly less than 0.60 in no fertilizer input treatment, indicating t serious N deficiency. The NNI of rice was between 0.60 and 1.0, little was less than 0.60, and a little was greater than 1.0 in the normally fertilized fields. In the fields with nitrogen-enhancing fertilization treatment, the NNI of rice was more than 1.0. The NNI estimation result (Fig. 5b) in the

Table 5
The R^2 and RMSE in the estimation of NNI using machine learning algorithms.

ML		Tillering	Early jointing	Late jointing	Booting	Flowering	Filling	Maturity
AB	R^2	0.83	0.64	0.52	0.79	0.45	0.80	0.52
	RMSE	0.09	0.12	0.18	0.13	0.13	0.07	0.09
ANN	R^2	0.50	0.72	0.50	0.53	0.58	0.80	0.55
	RMSE	0.20	0.10	0.17	0.20	0.20	0.08	0.16
KNN	R^2	0.50	0.50	0.33	0.55	0.42	0.56	0.43
	RMSE	0.21	0.13	0.19	0.19	0.08	0.09	0.07
PLSR	R^2	0.26	0.64	0.53	0.35	0.37	0.80	0.66
	RMSE	0.20	0.11	0.15	0.21	0.11	0.07	0.07
RF	R^2	0.95	0.96	0.96	0.94	0.88	0.97	0.89
	RMSE	0.05	0.05	0.07	0.07	0.05	0.03	0.03
SVM	R^2	0.36	0.75	0.48	0.25	0.24	0.78	0.63
	RMSE	0.24	0.10	0.15	0.24	0.16	0.08	0.06

Note: ML, machine learning; AB, adaptive boosting; ANN, artificial neural network; KNN, K-nearest neighbor; PLSR, partial least squares regression; RF, random forest; SVM, support vector machine

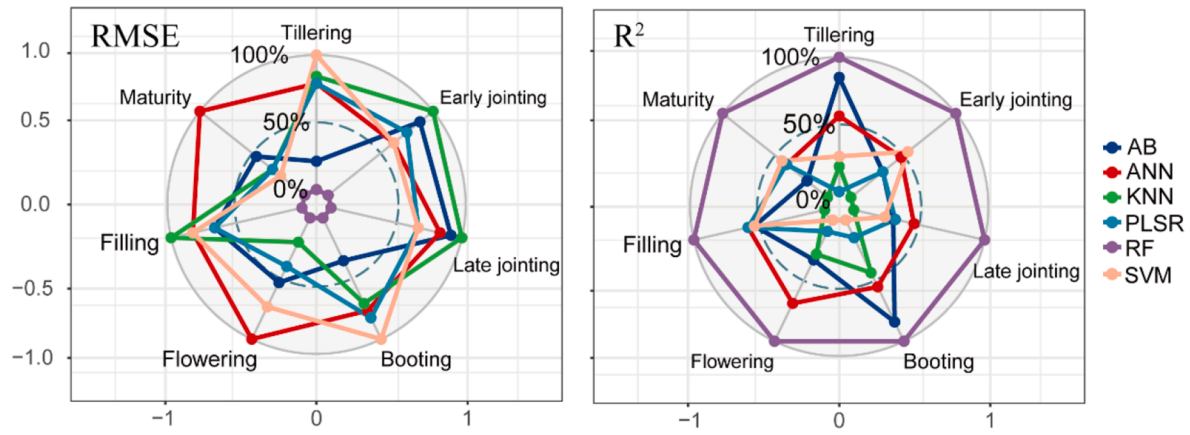

Fig. 2. Testing of the ML for the estimation of rice NNI at different growth period. R^2 and RMSE were the results from 1000-time dataset splitting.

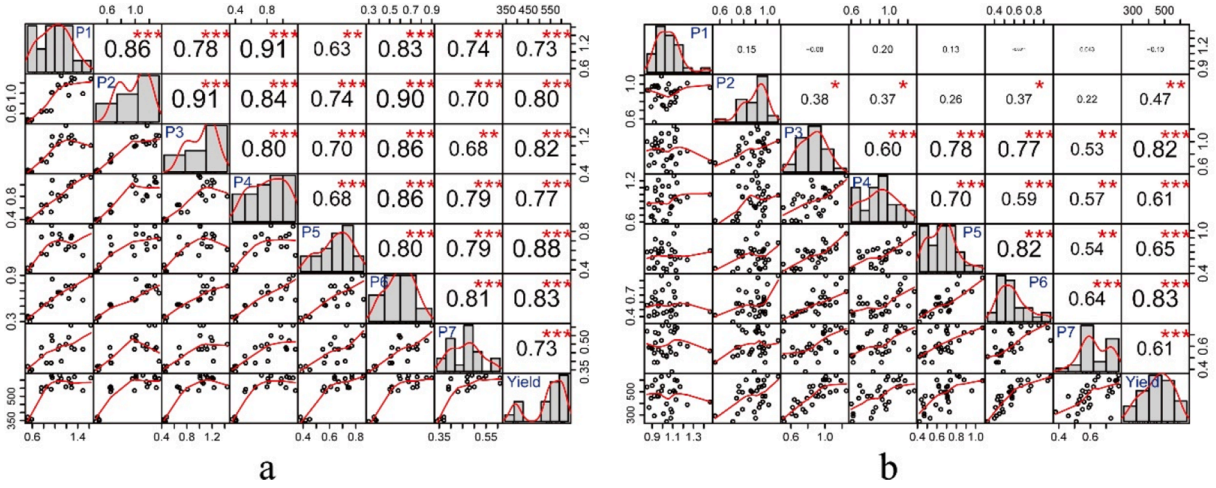

Fig. 3. Correlation analysis of yield with NNI at each period (a; results of Pukou experiment area; b; results of Luhe experiment area(P1, NNI at tillering stage; P2, NNI at early jointing stage; P3, NNI at late jointing stage; P4, NNI at booting stage; P5, NNI at flowering stage; P6, NNI at filling stage; P7, NNI at maturity stage). * 10% level of significance with p-values between 0.05 and 0.1; ** 5% level of significance with p-values between 0.01 and 0.05; *** 1% level of significance of significance with p-values less than 0.01.

Luhe experimental field showed that there was more variability of rice NNI in the same treated field, and some NNI were greater than 1 while some other were less than 0.40.

The validation results were shown in Fig. 6. It was found that the validation accuracy of the estimation results in the Pukou experimental field was relatively high with R^2 of 0.93, RMSE of 0.086, respectively (Fig. 6a), while in the Luhe experimental field the R^2 and RMSE were 0.74 and 0.22, respectively (Fig. 6b). The plot was uniform in Pukou experimental field due to smaller scale, while the Lukhe experimental area was a large relatively large scale, which resulted in the difference in validations. Totally, the estimated values of NNI showed high accuracy using RF algorithm with R^2 of 0.72 and RMSE of 0.209 (Fig. 6c), indicating that RF algorithm was suitable to estimate rice NNI.

4. Discussion

4.1. Feasibility of using UAV to estimate rice NNI

By analyzing the experimental data and UAV RGB image data obtained from two different experimental fields, it was proved that some VIs extracted from RGB images showed good correlation with NNI, and thus could be used to estimate NNI. However, due to the different performance of VIs on NNI in different growing periods, it was complicated to establish general models between different VIs and NNI, and the accuracy of simple linear regression models was not good enough. Therefore, ML algorithms were needed in this purpose, which could combine various VIs with rice NNI to build a nonlinear estimation model to improve the estimation accuracy and reduce the workload (Singh et al., 2016). Moreover, the estimation of rice NNI using the RF algorithm was good during the entire growth period, and the RF model established in this study could be used for the estimation of aboveground NNI of rice at the field scale. There were many research findings about the monitoring of important crop growth parameters using UAVs, such as leaf area index, dry biomass, chlorophyll content, and nitrogen concentration status, etc. (Cen et al., 2019; Zheng et al., 2019), which further validated the feasibility our results. Compared with the traditional method of measuring rice NNI in the laboratory, this method demonstrated the advantages of low cost and timeliness, and compared with the handheld sensors, rice NNI monitoring over a larger area was achieved using UAVs. Therefore, it was potential to estimate rice NNI using VIs extracted from UAV RGB images.

4.2. Optimization of machine learning algorithms

In this study, one of the objectives was to compare the different machine learning models for estimating rice NNI and to select the optimal estimation model. Six different ML algorithms (AB, ANN, KNN, PLSR, RF, and SVM) were used combined with UAV-VIs and measured

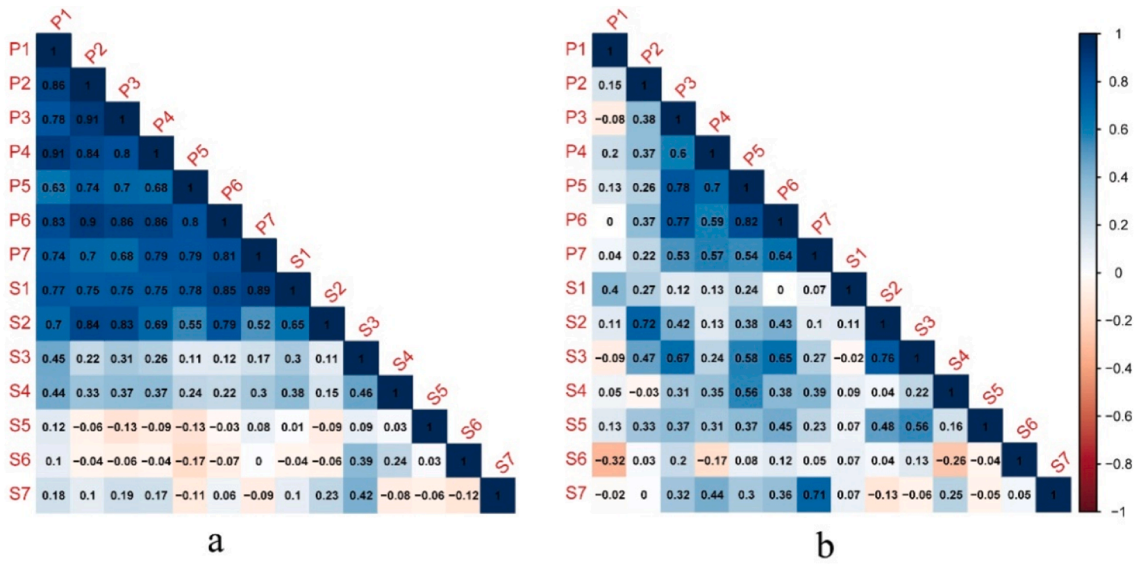

Fig. 4. Matrix of the correlation coefficient between the NNI and AN at different growth period (a; results of Pukou experiment area; b; results of Luhe experiment area(P1, NNI at tillering stage; P2, NNI at early jointing stage; P3, NNI at late jointing stage; P4, NNI at booting stage; P5, NNI at flowering stage; P6, NNI at filling stage; P7, NNI at maturity stage; S1, AN at tillering stage; S2, AN at early jointing stage; S3, AN at late jointing stage; S4, AN at booting stage; S5, AN at flowering stage; S6, AN at filling stage; S7, AN at maturity stage).

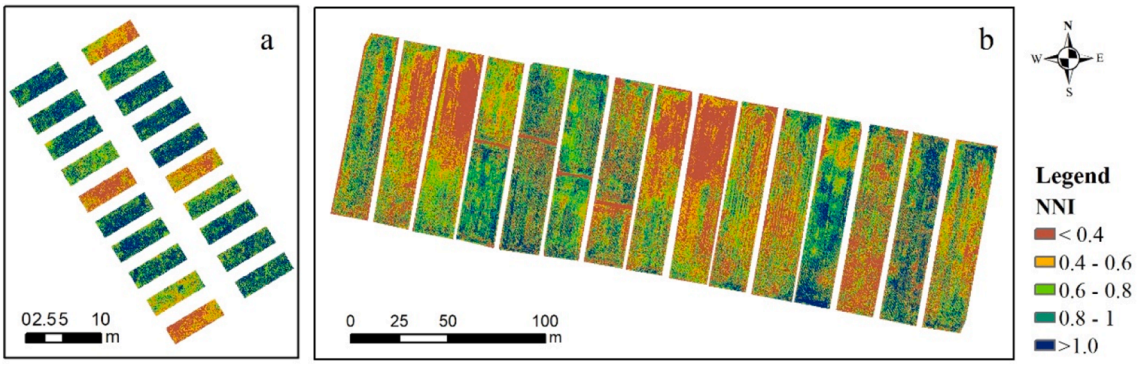

Fig. 5. NNI predicted map of rice at the early jointing stage based on UAV images and RF model (a, NNI predicted map of Pukou experimental field; b, NNI predicted map of Luhe experimental field).

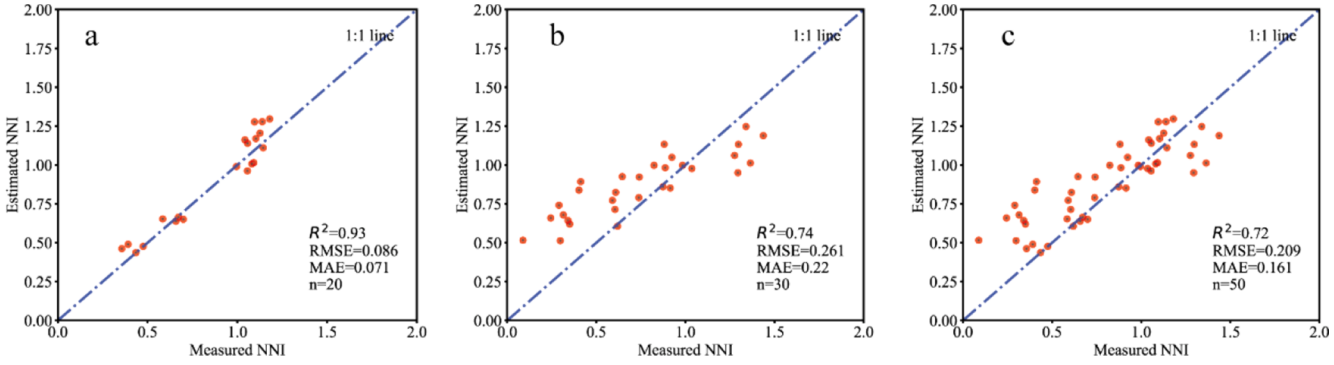

Fig. 6. Validation plots of estimated and measured rice NNI at the early jointing stage based on UAV images and RF model: a: validation results of Pukou experimental field; b: validation results of Luhe experimental field; c: validation results of all measured values and estimated values of two experimental fields.

NNI to achieve estimating rice NNI at the field scale. The validation results showed that the RF model consistently performed the best among all algorithms (Table 5 and Fig. 2), with R^2 greater than 0.88 and RMSE less than 0.21 throughout the growth period. RF was a learning method that integrated multiple decision trees, efficiently processing large-scale information with the ability to obtain a good fit with less noise. The other ML algorithms, which were not well validated on the test dataset, the validation accuracy of the algorithms was not as high as that of the RF algorithms. The AB algorithm at the tillering, booting and filling stages, the ANN and PLSR algorithms at the filling stage, and the SVM at

the early jointing and filling stages performed better, with validation R^2 of more than 0.70. Although these models showed good validation accuracy at some growth periods, they were not stable enough and thus were not recommended in the practical estimation of rice NNI. The KNN algorithm performed the worst among all algorithms, with validation R^2 less than 0.60 for all growth periods. Because the KNN algorithm was a simply constructed model with different sensitivities to the input parameters during training, it might lead to relatively poor prediction results; therefore, the RF algorithm used in this study was the optimal algorithm.

4.3. Relationship between rice NNI and soil AN

Many studies have been conducted using UAV to monitor the aboveground nitrogen content of crops, and the actual measured NNI was applied to guide fertilizer application in the field (Shi et al., 2021), but few studies have been conducted in terms of analyzing soil AN. The traditional method of obtaining soil AN was based on laboratory testing, the purpose of this study is indirectly guiding rice precision fertilization through UAVs by establishing the correlation between rice NNI and soil AN in a preliminary way. By analyzing the relationship between NNI and soil AN at each growth period, the results of two different experimental fields indicated that there was a significant correlation between NNI and AN at the early jointing stage. This finding provides some implications for the formulation of fertilization decisions. As shown in Fig. 3, the relationships between NNI and yield in both two experimental fields were highest at the late jointing and the filling stage, indicating that the high or low NNI of rice during these two growth periods could affect the yield status. If fertilizer was input at the late jointing stage, there would be a certain lag in nutrient uptake and transformation in rice. Therefore, to increase nitrogen use efficiency, fertilizer management should be considered before late jointing stage.

It was timely and reasonable for us to find out the nitrogen status through monitoring rice NNI in the early jointing stage, and thus the guidance of top dressing; the idea of using consumer UAV for monitoring rice NNI and guiding rice fertilization provided a convenient and low cost method for precise management of fertilization. However, the rice varieties were not considered, which showed limitation in practice. In order to make the results more adaptable, the varietal parameters and regional variations of rice need be considered in future studies.

5. Conclusions

Eleven VIs were extracted from UAV-RGB images at different growing period, and the NNI was calculated by combining the measured N concentration of rice at the corresponding period. The correlation analysis proved that most of the UAV-VIs were significantly correlated with the rice NNI at the corresponding period, but the UAV-VIs with the strongest correlation varied at different period. The NNI of different growth periods were predicted by six ML algorithms using UAV-VIs, and the validation results showed that the RF algorithm was the optimal algorithm for predicting NNI with R^2 in the range of 0.88–0.97, and RMSE in the range of 0.03–0.07. Meanwhile, there was a significant correlation between rice NNI and yield with R^2 of more than 0.80 at the late jointing and filling stage, and at the early jointing, there was a stable correlation between rice NNI and soil AN; therefore, the rice NNI could benefit the precise fertilization and nutrient utilization.

CRediT authorship contribution statement

Zhengchao Qiu: Data curation, Investigation, Conceptualization, Software, Writing – original draft. **Fei Ma:** Visualization, Investigation. **Zhenwang Li:** Software, Validation. **Xuebin Xu:** Investigation, Software. **Haixiao Ge:** Investigation, Data curation. **Changwen Du:** Conceptualization, Methodology, Supervision, Writing – review & editing, Funding acquisition.

Declaration of Competing Interest

The authors declare that they have no known competing financial interests or personal relationships that could have appeared to influence the work reported in this paper.

Acknowledgements

This research was funded by the National Key Research and Development Program of China (2018YFE0107000), and Key Research and Development Program of Shandong Province (2019JZZY010713).

References

Bendig, J., Yu, K., Aasen, H., Bolten, A., Bennertz, S., Broscheit, J., Gnyp, M.L., Bareth, G., 2015. Combining UAV-based plant height from crop surface models, visible, and near infrared vegetation indices for biomass monitoring in barley. Int. J. Appl. Earth Obs. Geoinf. 39, 79–87. https://doi.org/10.1016/j.jag.2015.02.012.

Cen, H.Y., Wan, L., Zhu, J.P., Li, Y.J., Li, X.R., Zhu, Y.M., Weng, H.Y., Wu, W.K., Yin, W. X., Xu, C., Bao, Y.D., Feng, L., Shou, J.Y., He, Y., 2019. Dynamic monitoring of biomass of rice under different nitrogen treatments using a lightweight UAV with dual image-frame snapshot cameras. Plant Methods 15, 32. https://doi.org/10.1186/s13007-019-0418-8.

Cohan, J.P., Le Souder, C., Guicherd, C., Lorgeou, J., Du Cheyron, P., Bonnefoy, M., Decarrier, A., Piraux, F., Laurent, F., 2019. Combining breeding traits and agronomic indicators to characterize the impact of cultivar on the nitrogen use efficiency of bread wheat. Field Crops Res. 242, 107588. https://doi.org/10.1016/j.fcr.2019.107588.

Fabbri, C., Mancini, M., dalla Marta, A., Orlandini, S., Napoli, M., 2020. Integrating satellite data with a nitrogen nutrition curve for precision top-dress fertilization of durum wheat. Eur. J. Agron. 120, 126148. https://doi.org/10.1016/j.eja.2020.126148.

Han, L., Yang, G.J., Dai, H.Y., Xu, B., Yang, H., Feng, H.K., Li, Z.H., Yang, X.D., 2019. Modeling maize above-ground biomass based on machine learning approaches using UAV remote-sensing data. Plant Methods 15, 10. https://doi.org/10.1186/s13007-019-0394-z.

Kerkech, M., Hafiane, A., Canals, R., 2020. Vine disease detection in UAV multispectral images using optimized image registration and deep learning segmentation approach. Comput. Electron. Agric. 174, 105446. https://doi.org/10.1016/j.compag.2020.105446.

Kogan, F.N., 1990. Remote sensing of weather impacts on vegetation in non-homogeneous areas. Int. J. Remote Sens. 11 (8), 1405–1419. https://doi.org/10.1080/01431169008955102.

Li, W., Niu, Z., Wang, C., Huang, W., Chen, H., Gao, S., Li, D., Muhammad, S., 2015. Combined use of airborne lidar and satellite GF-1 data to estimate leaf area index, height, and aboveground biomass of maize during peak growing season. IEEE J. Sel. Top. Appl. Earth Obs. Remote Sens. 8 (9), 4489–4501. https://doi.org/10.1109/JSTARS.460944310.1109/JSTARS.2015.2496358.

Louhaichi, M., Borman, M.M., Johnson, D.E., 2008. Spatially located platform and aerial photography for documentation of grazing impacts on wheat. Geocarto Int. 16 (1), 65–70. https://doi.org/10.1080/10106040108542184.

Lu, N., Zhou, J., Han, Z.X., Li, D., Cao, Q., Yao, X., Tian, Y.C., Zhu, Y., Cao, W.X., Xheng, T., 2019. Improved estimation of aboveground biomass in wheat from RGB imagery and point cloud data acquired with a low-cost unmanned aerial vehicle system. Plant Methods 15, 17. https://doi.org/10.1186/s13007-019-0402-3.

Ma, B.L., Zheng, Z., Pageau, D., Vera, C., Fregeau-Reid, J., Xue, A., Yan, W., 2017. Nitrogen and phosphorus uptake, yield and agronomic traits of oat cultivars as affected by fertilizer N rates under diverse environments. Nutr. Cycl. Agroecosyst. 108 (3), 245–265. https://doi.org/10.1007/s10705-017-9848-8.

Meyer, G.E., Neto, J.C., 2008. Verification of color vegetation indices for automated crop imaging applications. Comput. Electron. Agric. 63 (2), 282–293. https://doi.org/10.1016/j.compag.2008.03.009.

Nelson, D.W., Sommers, L.E., 1973. Determination of total nitrogen in plant material. Agron. J. 65, 109–112. https://doi.org/10.2134/agronj1973.00021962006500010033x.

Possoch, M., Bieker, S., Hoffmeister, D., Bolten, A., Schellberg, J., Bareth, G., 2016. Multi-temporal crop surface models combined with the RGB vegetation index from UAV-based images for forage monitoring in grassland. Int. Arch. Photogrammetry, Remote Sens. Spatial Inform. Sci. 41, 991–998. https://doi.org/10.5194/isprsarchives-XLI-B1-991-2016.

Qi, J., Chehbouni, A., Huete, A.R., Kerr, Y.H., Sorooshian, S., 1994. A Modified soil adjusted vegetation index. Remote Sens. Environ. 48 (2), 119–126. https://doi.org/10.1016/0034-4257(94)90134-1.

Saberioon, M.M., Gholizadeh, A., 2016. Novel approach for estimating nitrogen content in paddy fields using low altitude remote sensing system. Int. Archives Photogrammetry, Remote Sens. Spatial Inform. Sci. 41, 1011–1015. https://doi.org/10.5194/isprsarchives-XLI-B1-1011-2016.

Sankaran, S., Khot, L.R., Espinoza, C.Z., Jarolmasjed, S., Sathuvalli, V.R., Vandemark, G. J., Miklas, P.N., Carter, A.H., Pumphrey, M.O., Knowles, N.R., Pavek, M.J., 2015. Low-altitude, high-resolution aerial imaging systems for row and field crop phenotyping: a review. Eur. J. Agron. 70, 112–123. https://doi.org/10.1016/j.eja.2015.07.004.

Scornet, E., 2015. Random forests and kernel methods. IEEE Trans. Inf. Theory 62 (3), 1485–1500. https://doi.org/10.1109/TIT.2016.2514489.

Shi, P., Wang, Y., Xu, J., Zhao, Y., Yang, B., Yuan, Z., Sun, Q., 2021. "Rice nitrogen nutrition estimation with RGB images and machine learning methods. Comput. Electron. Agric. 180, 105860. https://doi.org/10.1016/j.compag.2020.105860.

Singh, A., Ganapathysubramanian, B., Singh, A.K., Sarkar, S., 2016. Machine learning for high-throughput stress phenotyping in plants Trends. Plant Sci. 21 (2), 110–124. https://doi.org/10.1016/j.tplants.2015.10.015.

Tucker, C.J., 1979. Red and photographic infrared linear combinations for monitoring vegetation. Remote Sens. Environ. 8 (2), 127–150. https://doi.org/10.1016/0034-4257(79)90013-0.

Verrelst, J., Schaepman, M.E., Koetz, B., Kneubühler, M., 2008. Angular sensitivity analysis of vegetation indices derived from CHRIS/PROBA data. Remote Sens. Environ. 112 (5), 2341–2353. https://doi.org/10.1016/j.rse.2007.11.001.

Wang, Y., Shi, P.H., Zhang, G., Ran, J., Shi, W.M., Wang, D.J., 2016. A critical nitrogen dilution curve for japonica rice based on canopy images. Field Crops Res. 198, 93–100. https://doi.org/10.1016/j.fcr.2016.08.032.

Wang, Y., Wang, D.J., Zhang, G., Wang, J., 2013. Estimating nitrogen status of rice using the image segmentation of G-R thresholding method. Field Crops Res. 149, 33–39. https://doi.org/10.1016/j.fcr.2013.04.007.

Woebbecke, D.M., Meyer, G.E., Von Bargen, K., Mortensen, D.A., 1995. Color indices for weed identification under various soil, residue, and lighting conditions. Trans. ASAE 38, 259–269. https://doi.org/10.13031/2013.27838.

Wu, W., Ma, B., 2015. Integrated nutrient management (INM) for sustaining crop productivity and reducing environmental impact: a review. Sci. Total Environ. 512–513, 415–427. https://doi.org/10.1016/j.scitotenv.2014.12.101.

Yang, B.H., Wang, M.X., Sha, Z.X., Wang, B., Chen, J.L., Yao, X., Cheng, T., Cao, W.X., Zhu, Y., 2019. Evaluation of aboveground nitrogen content of winter wheat using digital imagery of unmanned aerial vehicles. Sensors (Basel) 19, 20. https://doi.org/10.3390/s19204416.

Zheng, H., Cheng, T., Zhou, M., Li, D., Yao, X., Tian, Y., Cao, W., Zhu, Y., 2019. Improved estimation of rice aboveground biomass combining textural and spectral analysis of UAV imagery. Precis. Agric. 20 (3), 611–629. https://doi.org/10.1007/s11119-018-9600-7.